Eridani: an active K dwarf and a planet hosting star?. The variability of its large-scale magnetic field topology

Sandra V. Jeffers, Pascal Petit, Stephen C. Marsden, Julien Morin, Jean-François Donati, Colin P. Folsom

A&A 569, A79 (2014)
DOI: 10.1051/0004-6361/201423725

Astronomy & Astrophysics

ϵ Eridani: an active K dwarf and a planet hosting star?

The variability of its large-scale magnetic field topology⋆

S. V. Jeffers[1], P. Petit[3,2], S. C. Marsden[4], J. Morin[1,5], J.-F. Donati[3,2], C. P. Folsom[3,2], and The BCool collaboration

[1] Institut für Astrophysik, Georg-August-Universität, Friedrich-Hund-Platz 1, 37077 Göttingen, Germany
e-mail: Jeffers@astro.physik.uni-goettingen.de
[2] Université de Toulouse, UPS-OMP, Institut de Recherche en Astrophysique et Planétologie, Toulouse, France
[3] Institut de Recherche en Astrophysique et Planétologie, 14 avenue Edouard Belin, 31400 Toulouse, France
[4] Computational Engineering and Science Research Centre, University of Southern Queensland, 4350 Toowoomba, Australia
[5] LUPM, UMR 5299, CNRS & Université Montpellier II, Place E. Bataillon, 34095 Montpellier Cedex 05, France

Received 27 February 2014 / Accepted 1 July 2014

ABSTRACT

The young K-dwarf ϵ Eridani is an example of a young active planet hosting star that has shown over long-term monitoring of its chromospheric emission to exhibit cyclic magnetic activity. In this paper, we investigate how ϵ Eridani's large-scale magnetic field geometry evolves over the timescale of its S-index cycle using spectropolarimetric observations and the technique of Zeeman-Doppler imaging. Our observations comprise six epochs secured over a time period of nearly seven years, with each almost yearly observational epoch showing a dramatic change in the large-scale magnetic field topology, with no stable regions. The poloidal field varies from strongly dipolar to mono-polar and the toroidal field is non-existent to begin with and then emerges to dominate the magnetic field energy before disappearing and re-emerging again. A potential cycle is detected in the poloidal field, but further observations are needed to confirm this.

Key words. magnetic fields – stars: activity – stars: magnetic field – starspots

1. Introduction

The young bright K-dwarf ϵ Eridani is well known as a solar analogue and an exoplanet host star that also has a debris disk (Greaves et al. 2005). It is well established to be magnetically active, from direct measurements of its magnetic field (Rueedi et al. 1997; Smith 1983) and the long-term monitoring of activity proxies such as the cores of Ca II H&K lines that show variable cyclic behaviour. From an analysis of the full Ca II H&K observational history over a period of 45 years starting with the Mount Wilson survey (Baliunas et al. 1995), Metcalfe et al. (2013) determined two coexisting three year and 13-year periods that evolve into an activity minimum state for seven years, followed by the re-emergence of only the three year period. In this paper we investigate how the large-scale magnetic field geometry evolves over the course of this three year cycle by monitoring the large-scale magnetic field topology of ϵ Eridani over six observational epochs spread over a period of nearly seven years.

As a planet hosting star, ϵ Eridani is considered to host a 1.55 ($\pm$0.24) $M_{\rm Jupiter}$ planet orbiting at 3.39 AU detected via the radial velocity technique (Hatzes et al. 2000). The existence of the planet could be questionable however because of the background jitter in the radial velocity data. In recent work, Anglada-Escudé & Butler (2012) re-analysed all high precision radial velocity data for ϵ Eridani along with new observations. They determined a planetary orbit that is inconsistent with the previously reported solutions of Hatzes et al. (2000), Butler et al. (2006), Benedict et al. (2006) and suggest that the long-term radial velocity variability of ϵ Eridani is likely to result from stellar activity cycles rather than from a tentative planet. Additionally, density inhomogenities and gaps in the surrounding debris disk have also been used to infer the existence of a second long-period planetary companion (Quillen & Thorndike 2002; Backman et al. 2009).

The presence of a magnetic field can result in distortions in the shape of a star's spectral lines and consequently can result in spurious distortions in the star's radial velocity profile (Reiners et al. 2013; Jeffers et al. 2014). For example, it can induce spectral line broadening via the Zeeman effect, can be responsible for cool/hot spots, and can induce convective blueshifts. By reconstructing the topology of the large-scale magnetic field, and not just relying on the proxies of activity, we are able to gain a more in-depth understanding of the causes of the radial velocity variations. In this paper, we investigate the evolution of the large-scale magnetic topology of ϵ Eridani over six epochs spanning seven years of observations using the technique of Zeeman-Doppler imaging. In Sect. 2, we describe the observations and data analysis, followed by the determination of the longitudinal magnetic field and activity proxies in Sect. 3. In Sect. 4, we present the magnetic maps, and in Sect. 5 we discuss the implications of our results. In a follow-up paper, we will quantify the impact that the reconstructed magnetic field has on stellar jitter levels and consequently the detection of exoplanets. This paper is part of the Bcool[1] collaboration investigating the magnetic activity of low-mass stars.

⋆ Based on observations made with Telescope *Bernard Lyot* (TBL, Pic du Midi, France) of the Observatoire Midi-Pyrenees, which is operated by the Institut National des Sciences de l'Univers of the Centre National de la Recherche Scientifique (CNRS) of France.

[1] http://bcool.ast.obs-mip.fr

Table 1. Stellar parameters.

Parameter	Value	Reference
Magnitude	$V = 3.7$	
Spectral type	K2V	Valenti & Fischer (2005)
Distance	3.2 pc	van Leeuwen (2007)
Effective temperature	5146^{+31}_{-31} K	Valenti & Fischer (2005)
Mass ($M_\odot$)	$0.856^{+0.006}_{-0.008}$	Valenti & Fischer (2005)
Radius ($R_\odot$)	0.74 ± 0.01	Baines & Armstrong (2012)
$v \sin i$ (km s^{-1})	$2.4^{+0.04}_{-0.04}$	Valenti & Fischer (2005)
$P_{\rm rot}$ (day)	11.68	Rueedi et al. (1997)
Inclination	$46 \pm 2°$	this work
Age	440 Myr	Barnes (2007)

2. Stellar parameters

The stellar parameters of ϵ Eridani are shown in Table 1. The inclination is determined from the value of ϵ Eridani's radius measured using interferometry, its $v \sin i$ and rotation period. The age of 440 Myr is determined from its rotation period by Barnes (2007), though it should be noted that other methods yield much older values. A full discussion on the various methods used to determine ϵ Eridani's age is provided by Janson et al. (2008).

3. Observations and data analysis

The observations were secured using the fibre-fed high-resolution echelle spectropolarimeter NARVAL at the Telescope *Bernard Lyot*, France (Aurière 2003) as part of the BCool long-term programme. NARVAL has a spectral resolution $R = 65\,000$ and a wavelength range of 370 nm to 1000 nm. Each circularly polarised profile, comprises four sub-exposures, with different modulator angles. The instrumental setup, observing and data reduction procedure has previously been described in detail by Petit et al. (2008).

We observed ϵ Eridani at six different epochs (January 2007 (2007.08), January 2008 (2008.09), January 2010 (2010.04), October 2011 (2011.81), October 2012 (2012.82), and October 2013 (2013.75)). The observations are summarised in Table 2. The data were reduced using the automatic data reduction package LIBRE-ESPRIT which has been specifically adapted to reducing both Stokes I (unpolarised) and Stokes V (circularly polarised) NARVAL and HARPSpol (High Accuracy Radial Velocity Planet Searcher) data. More details can be found in Donati et al. (1997). The HARPSpol data for epoch 2010.04 were previously published by Piskunov et al. (2011).

The signal-to-noise ratio (S/N) is not sufficiently high in the reduced spectra to detect Stokes V signatures directly. All Stokes I and Stokes V reduced spectra were processed using least-squares deconvolution (LSD; Donati et al. 1997). The multi-line technique LSD extracts the information contained in each spectral line, resulting in one high S/N spectral profile for each observation. The line mask was downloaded from the VALD atomic database for a star with: $T_{\rm eff} = 5000$ K, $\log g = 4.5$, a depth threshold of 0.1 and log(M/H) = 0.1 and containing 12 220 lines. This line mask was applied to each spectra resulting in a step size of 1.8 km s^{-1} in the LSD profile, as defined by the resolving power of NARVAL. For the HARPSpol data the step size was 1.1 km s^{-1}. The average S/N of the Stokes V profile after LSD was computed to be 41 800 in 2007.08, 55 200 in 2008.09, 49 300 in 2010.04, 61 900 in 2011.81, 44 600 in 2012.82, and 69 000 in 2013.75. More details on the application of LSD to the BCool sample is provided by Marsden et al. (2014).

Table 2. Journal of observations.

Date	Julian date (–2 454 000)	UT	Phase	Exp. time (s)	LSD *S/N*
		2007.08			
21 Jan. 07	122.254	18:06:06	0.777	480	34192
26 Jan. 07	127.315	19:33:23	1.210	480	29613
27 Jan. 07	128.311	19:27:58	1.296	480	40211
01 Feb. 07	133.325	19:48:30	1.725	480	45227
03 Feb. 07	135.315	19:34:14	1.895	480	52715
08 Feb. 07	140.328	19:52:10	2.324	480	48832
		2008.09			
19 Jan. 08	485.378	21:04:29	0.866	800	37097
21 Jan. 08	487.303	19:16:04	1.031	800	53813
22 Jan. 08	488.319	19:39:00	1.118	800	60782
23 Jan. 08	489.323	19:44:55	1.204	800	55648
24 Jan. 08	490.343	20:13:51	1.291	800	60957
25 Jan. 08	491.326	19:49:41	1.375	800	51066
26 Jan. 08	492.325	19:48:31	1.461	800	48932
27 Jan. 08	493.337	20:05:38	1.548	800	44772
28 Jan. 08	494.382	21:09:47	1.637	800	50639
29 Jan. 08	495.350	20:24:34	1.72	800	46596
02 Feb. 08	499.347	20:20:14	2.062	800	59853
04 Feb. 08	501.330	19:55:40	2.232	800	59604
05 Feb. 08	502.329	19:54:10	2.318	800	57201
06 Feb. 08	503.329	19:54:01	2.403	800	54587
09 Feb. 08	506.339	20:07:55	2.661	800	54432
10 Feb. 08	507.284	18:48:18	2.742	800	73519
11 Feb. 08	508.342	20:12:04	2.832	800	59739
12 Feb. 08	509.347	20:19:22	2.918	800	55095
13 Feb. 08	510.343	20:14:25	3.004	800	52639
14 Feb. 08	511.350	20:24:21	3.090	800	56040
15 Feb. 08	512.341	20:11:29	3.175	800	66723
		2010.04			
02 Jan. 10*	1199.61	2:40:22	0.016	760	60184
03 Jan. 10*	1200.59	2:16:20	0.101	760	68064
04 Jan. 10*	1201.66	3:43:31	0.191	1159	72688
05 Jan. 10*	1202.60	2:21:34	0.272	1160	74760
06 Jan. 10*	1203.55	1:18:40	0.354	1160	78127
07 Jan. 10*	1204.57	1:45:29	0.441	1000	84945
08 Jan. 10*	1205.60	2:20:28	0.529	960	77337
09 Jan. 10*	1206.57	1:47:16	0.613	960	80801
10 Jan. 10*	1207.62	2:54:04	0.702	960	70031
12 Jan. 10*	1209.56	1:29:46	0.868	960	83421
13 Jan. 10*	1210.59	2:11:49	0.957	960	82241
14 Jan. 10*	1211.58	1:56:52	1.041	1360	63316
		2011.81			
01 Oct. 11	1836.62	2:51:18	0.555	800	76183
03 Oct. 11	1838.63	3:13:32	0.727	800	76051
08 Oct. 11	1843.62	2:49:39	1.154	800	59418
10 Oct. 11	1845.50	23:58:04	1.315	800	51546
11 Oct. 11	1846.52	0:23:47	1.402	800	33388
15 Oct. 11	1850.51	0:17:34	1.744	800	76004
08 Nov. 11	1874.46	23:01:20	3.795	800	48678
10 Nov. 11	1876.59	2:07:37	3.977	800	65801
11 Nov. 11	1877.55	1:07:36	4.059	800	60304
16 Nov. 11	1882.53	0:50:05	4.486	800	71653

Notes. Phase = 0 is defined as 2 454 101.5 and is used for all epochs, with subsequent epochs taking phase = 0 as an integer number of cycles from this value. * Indicates data previously published by Piskunov et al. (2011).

Table 2. continued.

Date	Julian date	UT	Phase	Exp time (s)	LSD *S/N*
		2012.82			
01 Oct. 12	2202.53	0:41:57	0.883	480	48743
02 Oct. 12	2203.53	0:41:39	0.968	480	56037
04 Oct. 12	2205.55	1:14:24	1.141	480	48443
05 Oct. 12	2206.54	0:56:55	1.226	480	46065
13 Oct. 12	2214.49	23:45:32	1.907	480	26338
23 Oct. 12	2224.61	2:41:42	2.773	480	39967
28 Oct. 12	2229.54	0:52:29	3.195	480	43904
29 Oct. 12	2230.54	0:51:02	3.280	480	57203
31 Oct. 12	2232.51	0:16:47	3.450	480	49398
06 Nov. 12	2238.55	1:10:09	3.966	960	45407
12 Nov. 12	2244.50	24:04:19	4.476	480	42585
14 Nov. 12	2246.47	23:17:48	4.645	480	48843
22 Nov. 12	2254.48	23:20:27	5.330	480	28024
		2013.75			
19 Sep. 13	2555.63	3:09:32	0.114	800	68299
20 Sep. 13	2556.64	3:15:11	0.200	800	78657
21 Sep. 13	2557.63	3:07:22	0.285	800	76087
24 Sep. 13	2560.63	3:10:27	0.542	800	74820
06 Oct. 13	2572.6	2:18:41	1.567	800	68146
08 Oct. 13	2574.6	2:20:18	1.738	800	78641
09 Oct. 13	2575.58	1:49:47	1.822	800	74495
10 Oct. 13	2576.52	0:34:53	1.903	800	43438
11 Oct. 13	2577.6	2:24:42	1.995	800	61050
12 Oct. 13	2578.55	1:11:40	2.076	800	72240

4. Rotational variation of B_l, Ca II H&K and H_α

In this section, we determine the most commonly used magnetic field proxies to ascertain how they vary as a function of stellar rotation (and consequently with the reconstructed magnetic field topology) and with each observational epoch. The methods follow those of Marsden et al. (2014) for the Bcool snapshot survey and are briefly summarised here.

4.1. Longitudinal magnetic field

The stellar magnetic field averaged over the visible stellar hemisphere is estimated from the LSD profiles using the centre of gravity technique described by Rees & Semel (1979) and implemented by Marsden et al. (2014). The line-of-sight projection of the magnetic field B_l (and often referred to as B_z in other works), integrated over the stellar disk, can be determined from the Stokes I and V profiles by:

$$B_l = -2.14 \times 10^{11} \frac{\int v V(v) \mathrm{d}v}{\lambda_0 g c \int (I_c - I(v)) \mathrm{d}v} \quad (1)$$

where B_l is in Gauss, λ is the mean wavelength of the LSD profile in nm, g is the Lande factor, c is the speed of light, and I_c is the continuum level of the intensity profile and is normalised to 1.0. The Lande factor is set to 1.2 and the mean wavelength of the LSD profile is 560 nm. The longitudinal magnetic field is computed for all epochs of this analysis over a velocity span of 34 km s^{-1}, and the results are shown in Fig. 1. The result clearly shows a variation of the longitudinal magnetic field, including sign changes, as a function of stellar rotation indicating a non-axisymmetric distribution of surface magnetic fields.

4.2. Chromospheric emission – Ca II H&K

To determine the Ca II H&K S-values, we follow the method previously described by Morgenthaler et al. (2012) and Marsden et al. (2014). The flux in the line cores is determined by using two triangular band passes of width 0.1 nm, centred on the Ca II H (393.3663 nm) and Ca II K (396.8469 nm) line cores. Two continuum band passes R and V centred at 400.107 nm and 390.107 nm are used for the continuum flux. To match the Mount Wilson values, we apply the coefficients α, β, γ, δ, and ϵ in the form:

$$\mathrm{S_{index}} = (\alpha \mathrm{H} + \beta \mathrm{K})/(\gamma V + \delta R) + \epsilon. \quad (2)$$

The coefficients for the NARVAL spectrograph were computed by Marsden et al. (2014) using least-squares fitting to be: α = 12.873, β 2.502, γ 8.877, δ 4.271, ϵ 1.183×10^{-3}. The S-index for each epoch of observations is plotted in Fig. 1, top panel. There is a clear variability of the S-index with the stellar rotation period at all observational epochs. The long-term evolution of S-index for ϵ Eridani has been investigated by Metcalfe et al. (2013), where the distribution of values calculated for the epochs of this analysis are fully consistent with their long-term cyclic variations. The long-term variation of S-index over the epochs of this analysis is shown in Fig. 2, with an overplotted sinusiod matching the S-index values of Metcalfe et al. (2013).

4.3. Chromospheric emission – Ca IRT

Additionally, the Ca infrared triplet (IRT) activity proxy was determined using the Ca IRT lines at 849.802 nm (ca1), 854.209 nm (ca2), and 866.214 nm (ca3) using the equation (Marsden et al. 2014):

$$\mathrm{Ca_{IRT\text{-}index}} = \frac{(F_{\mathrm{ca1}} + F_{\mathrm{ca2}} + F_{\mathrm{ca3}})}{(F_{\mathrm{v}} + F_{\mathrm{r}})} \quad (3)$$

where $F_{\mathrm{ca1}}, F_{\mathrm{ca2}}$ and F_{ca3} are the fluxes of the IRT lines measured in 0.2 nm rectangular band-pass centred on the respective Ca IRT line. The values F_{v} and F_{r} are the fluxes in 0.5 nm rectangular band-passes centred on the two continuum points 847.58 nm, and 870.48 nm, located either side of the Ca IRT lines. The results, as a function of rotation period, are summarised in the lower panel of Fig. 1 for each observational epoch.

4.4. The H_α index

The variability in H_α is measured following the method of Gizis et al. (2002) and implemented by Morgenthaler et al. (2012). The H_α index is defined as

$$N_{\mathrm{H}\alpha} = \frac{F_{\mathrm{H}\alpha}}{C_{\mathrm{red}} - C_{\mathrm{blue}}} \quad (4)$$

where the line core, $F_{\mathrm{H}\alpha}$ is the flux in a rectangular band-pass between 656.10 nm and 656.46 nm, with the continuum band passes taken to be from 656.62–656.84 nm on the red side, C_{red}, and 655.77–656.0 nm on the blue side, C_{blue}. The results as a function of rotation period for each epoch of this analysis are shown in the lower panel of Fig. 1 for each observational epoch.

5. Large-scale magnetic field geometry

Synthetic Stokes V and I profiles are computed from a model of the stellar surface with local Stokes V or Stokes I profile.

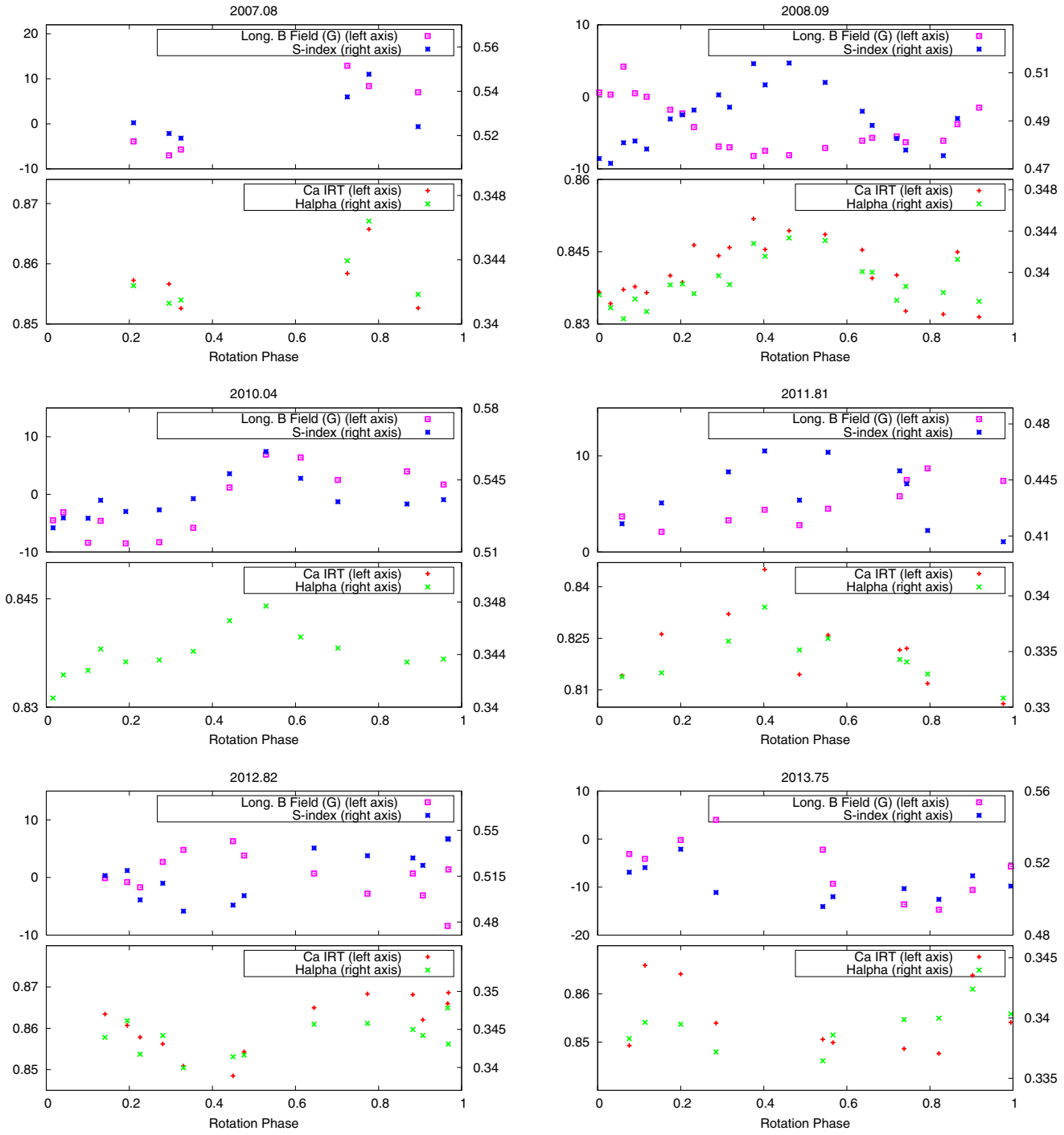

Fig. 1. For each epoch of observation, the variation of the longitudinal magnetic field (in Gauss, *upper panel*) and the variation of the magnetic proxies Ca II H&K (*upper panel*); Ca IRT-index and H_α-index (*lower panel*) as a function of stellar rotation phase. The S-index values for the Ca II H&K have been calibrated to match those from the Mount Wilson survey.

The modelled Stokes V profiles are then iteratively fitted to the observed Stokes V profiles using maximum entropy algorithm described by Skilling & Bryan (1984). The tomographic images of the large-scale magnetic field topology of ϵ Eridani were reconstructed using the stellar parameters shown in Table 1 and by assuming that the field geometry is projected onto a spherical harmonics frame (Donati et al. 2006), where the magnetic energy is decomposed into poloidal and toroidal components. A spherical harmonics expansion with $\ell_{\max} = 10$ was used as there was no improvement to the fits using larger values.

5.1. Magnetic maps

The resulting magnetic maps are shown in the central panels of Fig. 3, with the fits of the observed and modelled Stokes V LSD profiles at the side for 2007.08 (top row, left), 2008.09 (top row, right), 2010.04 (middle row, left), 2011.81 (middle row, right), 2012.82 (bottom row, left), and 2013.74 (bottom row, right). The magnetic field geometry is dominated by the poloidal and toroidal components with a negligible contribution from B_Θ (meridional component).

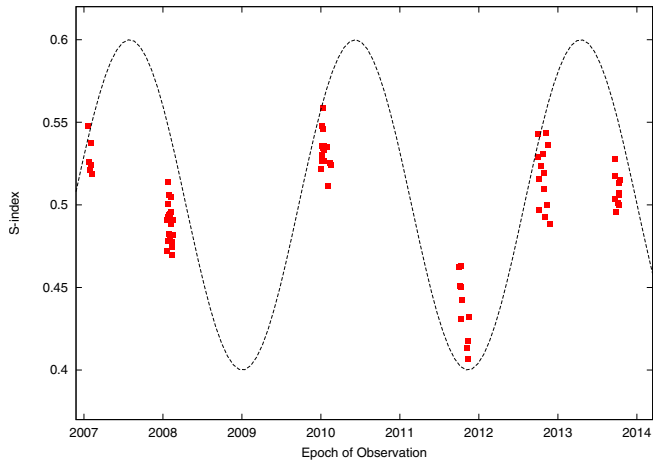

Fig. 2. Variation of S-index over the epochs of this analysis (points). Also shown (dashed line) is a sinusiod with period of 2.95 years as determined by Metcalfe et al. (2013).

5.1.1. Poloidal component

At all epochs, strong and large regions of negative and/or positive magnetic field are present in the radial field images. This varies from a predominately dipolar structure seen in 2007.08, with two distinct and large magnetic regions of opposite polarities; to a polar spot of negative field in 2008.09 and 2010.04 followed by a large region with positive polarity; returning to a large polar spot of negative field in 2012.82, with a weaker region of positive field at equatorial latitudes, and, finally; returning to a dipolar structure in 2013.75, although with a reversal of polarity of the large magnetic regions with a dominant negative region. The accuracy of the large-scale magnetic field structure could be reduced in 2007.08 due to a more sparse phase coverage for this epoch.

Evidence of strong poloidal magnetic field regions can also be directly seen in the Stokes V profiles, for epochs where the other magnetic field components are weak or non-existent. For example, in epoch 2007.08 the large region of negative polarity magnetic field in the radial field image can be clearly seen in the shape of the Stokes V profiles to the left of the image at phases 1.21, 1.296, and 2.324. Similarly, the constant polar magnetic field region reconstructed in 2008.09 is also apparent in the shape of the Stokes V profiles.

5.1.2. Toroidal component

The magnetic topology of ϵ Eridani shows a weak toroidal component in both 2007.08 and 2008.09, which then increases in strength to dominate over the poloidal component in 2010.04 with a strong region of negative field at low latitudes (this is a region of axisymmetric azimuthal field) before decreasing to a very weak field in 2011.81. The field increases again in 2012.82 in the form of a large equatorial negative magnetic region and is seen to almost disappear in 2013.75. The lack of any toroidal field in 2007.08, followed by the appearance of the toroidal field approximately three years later in 2010.04 and again in 2012.82 would indicate that there is no clear cyclic evolution of the polarity of the toroidal field component. We do note however, that the oscillation between strong and weak components could indicate a non-solar like dynamo process.

5.2. Magnetic energy

The magnetic energy that is contained in the different components of the magnetic maps was investigated where the magnetic energy in a component is calculated as being proportional to the square of that component integrated over the star. The poloidal component is defined by α and β terms Donati et al. (2006) (Eqs. (2)–(4)) and the axisymmteric component is defined by spherical harmonics with $m = 0$ modes. The poloidal and toroidal components of the magnetic energy are shown in Fig. 4 with the poloidal field sub-divided into its dipolar, quadrupolar, and octopolar components ($\ell \leq 3$). There is a clear temporal evolution of magnetic energy and how it is divided up into its components over the time span of our observations.

The poloidal component contains most of the energy at all observational epochs with the exception of 2010.04 where the toroidal component dominates (59%) and in 2012.82 where it is approximately the same (45%). These two maps have significantly axisymmetric fields, though the magnetic field is predominantly axisymmetric in the 2008.09 and 2012.82 maps.

5.3. Differential rotation

As the data were secured over a period of several weeks for epoch 2008.09, differential rotation is also included in the reconstruction of the magnetic field maps. This is equated as follows:

$$\Omega(\theta) = \Omega_{\rm eq} - {\rm d}\Omega \sin^2 \theta, \quad (5)$$

where $\Omega(\theta)$ is the rotation rate of the star at a latitude θ, $\Omega_{\rm eq}$ is the rotation rate of the equator, and dΩ is the difference in the rotation of the star at the equator and at the pole. Magnetic maps are reconstructed using a grid of $\Omega_{\rm eq}$ and dΩ values and where the minimum χ^2 value is taken as the differential rotation value (following the method of Petit et al. 2002). The values obtained for 2008 are $\Omega_{\rm eq} = 0.608$ rad d^{-1} and d$\Omega = 0.2$ rad d^{-1}, which translate into rotational periods for the equator of $P_{\rm eq} = 10.33$ d and the pole of $P_{\rm pole} = 15.4$ d. These values are in agreement with the values derived from photometric data from the MOST satellite of 11.35 days, 11.55 days for two different spots (Croll et al. 2006).

In practice, it was only possible to determine a reliable χ^2 minimum for the data from 2008.09. The other observational epochs did not contain sufficient rotational phase overlap to measure ϵ Eridani's differential rotation. The values of differential rotation measured in 2008.09 were applied to the other epochs of observations.

6. Discussion

6.1. Activity proxies

The proxies of magnetic activity, S-index (Ca II H&K), H$_\alpha$, and Ca II IRT, clearly show that the magnetic activity of ϵ Eridani varies with its rotational phase. Globally, there appears to be a correlation between the chromospheric proxies of activity for each epoch. There is a correlation of the S-index with the measurement of the longitudinal magnetic field at epochs 2007.08, 2010.04, 2013.75, anti-correlation in 2008.09, and in 2012.82, and no correlation in 2011.81. It should be noted however, that the longitudinal magnetic field values are considered to indicate the minimum strength of ϵ Eridani's magnetic field because the measurements are integrated over the visible stellar surface and do not account for flux cancellation. The rotational variation of

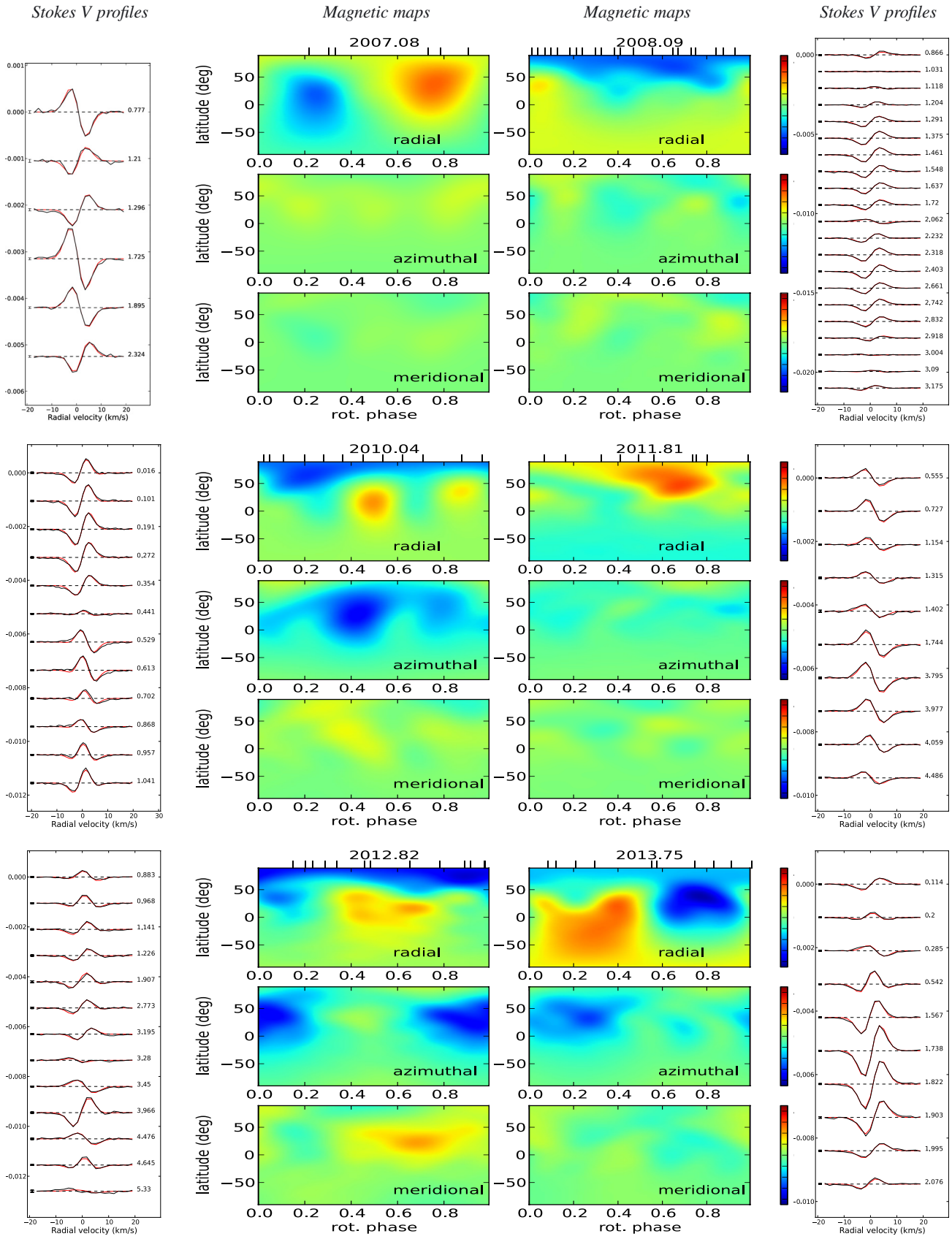

Fig. 3. Magnetic field maps of ϵ Eridani reconstructed for 2007.08, 2008.09, 2010.04, 2011.81, 2012.82, and 2013.75, shown with the Stokes V fits to the sides. For each image the magnetic field projection is shown in terms of poloidal (*upper*), toroidal (*middle*), and meridional (*lower*) field components, where red indicates positive polarity and blue negative polarity. The magnetic field strength is in Gauss where for each map the scale is identical (Bmax = 45 G). The tick marks at the top of each poloidal field map indicate the observational phases used to reconstruct the large-scale magnetic field geometry. Given that the inclination of ϵ Eridani is 46°, there is no information on the magnetic field topology in the lower 1/4 of each image. The Stokes V profiles are plotted separated by a constant value for clarity.

Table 3. Fraction of the large-scale magnetic energy reconstructed in the toroidal and poloidal field components; fraction of the poloidal field in the dipolar ($\ell = 1$), quadrupolar ($\ell = 2$), and octopolar ($\ell = 3$) components; and fraction of the energy stored in the axisymmetric component ($m = 0$).

Observational Epoch	Bmean	χ^2	Bmax (G)	Toroidal (% tot)	Poloidal (% pol)	Dipolar (% pol)	Quadrupolar (% pol)	Octopolar (% tot)	Axisymmetric	
2007.08	12 ± 1		28 ± 3	8 ± 2	92 ± 2	92 ± 1	6 ± 1	1 ± 1	16 ± 4	1.2
2008.09	10 ± 1		29 ± 6	6 ± 3	94 ± 3	64 ± 5	23 ± 1	8 ± 2	58 ± 12	1.2
2010.04	16 ± 4		39 ± 9	59 ± 5	41 ± 7	37 ± 12	38 ± 4	20 ± 6	72 ± 8	3.7
2011.81	10 ± 1		32 ± 1	26 ± 7	74 ± 8	65 ± 10	15 ± 3	10 ± 3	63 ± 10	1.9
2012.82	18 ± 3		42 ± 7	45 ± 8	55 ± 7	71 ± 3	16 ± 1	8 ± 1	59 ± 4	1.65
2013.75	20 ± 1		42 ± 2	22 ± 7	78 ± 9	85 ± 2	5 ± 1	6 ± 1	36 ± 1	2.5

Notes. The χ^2 values are those achieved in the reconstruction of the large-scale magnetic field for each epoch of observation.

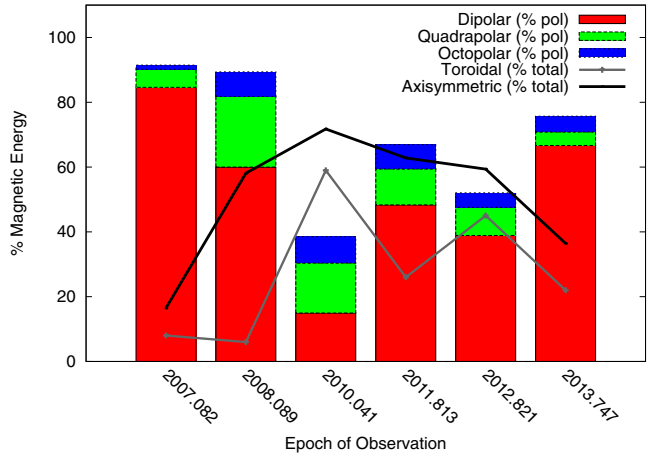

Fig. 4. Composition of the magnetic energy (higher order modes) for each epoch of this analysis. The total poloidal component is shown as a column stacked histogram in terms of its dipolar, quadrupolar, and octopolar components. The axisymmetric component is shown as a continuous black line and the toroidal component is shown as a continuous grey line.

the measured S-index indicates that the magnetic field structure on ϵ Eridani is complex. Since the chromospheric S-index measurement does not suffer from flux cancellation it provides a more direct indication of the complexity of the magnetic field structure.

The long-term variation of ϵ Eridani's S-index has been determined for over 45 years. Metcalfe et al. (2013) determined that there are two coexisting periods of three and 13 years, which went though a minimum state for seven years with only the three-year period emerging afterwards. The observations presented in this analysis span nearly seven years from 2007.08 to 2013.75, as summarised in Fig. 2. The global variations are in agreement with the long-term S-index trend reported by Metcalfe et al. (2013) for epochs up to 2012 and cover two S-index cycles. For epoch 2011.81 we were able to observe ϵ Eridani precisely at its S-index minimum, and we have yet to observe ϵ Eridani at its S-index maximum. At this stage, our time sampling is too short to thoroughly investigate an activity cycle of ~three years.

6.2. Large-scale magnetic field topology

The reconstructed toroidal field is highly variable over all observational epochs ranging from almost non-existent in 2007.08 and 2008.09 to strong negative regions at mid-latitudes in 2010.04, where it contains up to 60% of the total magnetic energy. This evolves into very weak magnetic field regions in 2011.81 and returns to a strong negative magnetic region in 2012.82 and is shown to weaken in 2013.75. The low strength and the rapid variations of the toroidal field, reconstructed at some epochs, are in contrast to the long stable rings of toroidal field that have been reconstructed on more rapidly rotating stars (for example HD 171488 Jeffers et al. 2011) or indeed the absence of toroidal field of low activity stars with rotation periods greater than 12 days (Petit et al. 2008).

The cyclic variation of ϵ Eridani's S-index has been shown by Metcalfe et al. (2013) to comprise both high and low amplitude peaks and troughs. Correlating the observational epochs of this analysis with this long-term monitoring, and as shown in Fig. 2, indicates that in 2007.08, the S-index value was almost at a maximum level for that particular low amplitude cycle, which reached a maximum approximately in 2007.5. By the time of the next observational epoch in 2008.09, the S-index value has started to decrease following Metcalfe et al. (2013), reaching a minimum in 2009.0 and increasing again to its next maximum in approximately 2010.5, indicating that activity in the magnetic map reconstructed at epoch 2010.04 is increasing. The very weak magnetic field reconstructed for epoch 2011.81 directly correlates with the activity minimum in S-index. By the next observational epoch in 2012.82, the S-index is increasing up to its maximum in 2013.5, and decreasing again in 2013.75. As noted by Rueedi et al. (1997) the magnetic field regions are predominantly in the form of plage regions, implying that we should expect to see such a correlation.

We also note that the presence of large regions of toroidal field in 2010.81 and 2012.82 are both epochs where ϵ Eridani's S-index was increasing. From Fig. 2, it would appear that 2007.08 is also associated with increasing values of ϵ Eridani's S-index, but the results of Metcalfe et al. (2013) show that this was a very low amplitude peak where the S-index values did not increase much more than the maximum value shown for 2007.082.

Additional spectropolarimetric data of ϵ Eridani in February 2011 were downloaded from the ESO archive. While there are insufficient Stokes V profiles to reliably reconstruct the large-scale magnetic field geometry of ϵ Eridani, the amplitude of the Stokes V profiles are significantly lower than for the other epochs of this analysis. As a first order approximation, this would indicate that ϵ Eridani was not as magnetically active at this time, which is surprising as at this epoch the S-index values were still decreasing after its maximum in 2010.5. This apparent lack of a consistent correlation of the S-index measurement with

the large-scale field may suggest that all magnetic elements on the stellar surface (contributing to S-index) do not behave like the large-scale field. This is not completely different from the Sun, for which active regions do not follow the large-scale field structure, but it is interesting to find something similar for faster rotators and their long-term evolution. This was also reported by Fares et al. (2009) for τ Boo, where the magnetic cycle derived from the large-scale field is much shorter than the magnetic cycle estimated from S-index measurements (Baliunas et al. 1995), and is also observed for HN Peg.

Other stars that exhibit clear magnetic cycles include the older F9 dwarf HD 78366 (age = 1 Gyr (chromospheric), $v \sin i$ = 3.9 km s^{-1}, rotation period =11.4 d) which shows a simple large-scale magnetic field geometry with clear cyclic behaviour in its poloidal field with a period of approximately three years and on the more rapidly rotating F7 dwarf τ Boo (Fares et al. 2009). The magnetic cycles on τ Boo (age = 1.6 to 2.3 Gyr, mass =1.34, $v \sin i$ = 15.0 km s^{-1} rotation period =3.0 d) have a period of two years with a global magnetic polarity reversal that is observed in all three components of the field. The poloidal component of the magnetic field also shows polarity switches from positive regions at polar latitudes and negative regions at lower latitudes to regions of opposite polarity.

More complex magnetic variability, similar to that observed on ϵ Eridani, has been observed in much older stars such as HD 190771 (Petit et al. 2009; Morgenthaler et al. 2011) (spectral type G5IV, age = 1.7 Gyr, $v \sin i$ = 4.3 km s^{-1}, rotation period =8.8 days). Over a period of three observational epochs each separated by approximately one year, HD 190771 shows polarity reversals first in its toroidal field component, which has most of the energy at the first epoch of observation, followed by a shift in magnetic energy to predominately poloidal field, and then polarity changes in its poloidal field. One of the surprising results is that ϵ Eridani's toroidal magnetic field can disappear and then reappear. Similarly, strong variations in the presence and intensity of the large-scale toroidal magnetic field regions have previously been observed in the slowly rotating star ξ Boo A (Morgenthaler et al. 2012) (spectral type G8 V, age = 1 Gyr, $v \sin i$ = 4.6 km s^{-1}, and rotation period =6.43 days), where the intensity of the magnetic field regions is noted to decrease by 50% over a period of six months. While ϵ Eridani's stellar parameters are quite similar to those of ξ Boo A, we do note that its age of 440 Myr (Barnes 2007, derived from its rotation period; see Janson et al. 2008, for a full discussion) is significantly younger, and its rotation period is approximately a factor of two longer. In general, cyclic behaviour has yet to be detected on stars that are much more magnetically active than ϵ Eridani as these stars tend to be younger and rotate much more rapidly, which could indicate that the stellar activity is highly variable and harder to detect (Jeffers & Donati 2008; Jeffers et al. 2011; Donati et al. 2003; Baliunas et al. 1995).

7. Summary

In this paper, we have reconstructed the large-scale magnetic field geometry of the young active K dwarf ϵ Eridani over seven years and comprising six observational epochs. The large-scale magnetic field geometry is shown to be highly variable, with no common features seen from one year to the next. Over the complete time-span of our observations, we potentially see a cyclic pattern, but we will need to obtain a higher temporal sampling to investigate the magnetic activity over ϵ Eridani's S-index cycle. In a future paper, we will determine how this highly variable magnetic field geometry can impact the detection of exoplanets.

Acknowledgements. S.V.J. acknowledges research funding by the Deutsche Forschungsgemeinschaft (DFG) under grant SFB 963/1, project A16. J.M.'s work in Göttingen was funded by a postdoctoral fellowship of the Alexander von Humboldt foundation. Part of this work was supported by the COST Action MP1104 "Polarization as a tool to study the Solar System and beyond".

References

Anglada-Escudé, G., & Butler, R. P. 2012, ApJS, 200, 15
Aurière, M. 2003, in EAS Pub. Ser. 9, eds. J. Arnaud, & N. Meunier, 105
Backman, D., Marengo, M., Stapelfeldt, K., et al. 2009, ApJ, 690, 1522
Baines, E. K., & Armstrong, J. T. 2012, ApJ, 744, 138
Baliunas, S. L., Donahue, R. A., Soon, W. H., et al. 1995, ApJ, 438, 269
Barnes, S. A. 2007, A&A, 669, 1167
Benedict, G. F., McArthur, B. E., Gatewood, G., et al. 2006, AJ, 132, 2206
Butler, R. P., Wright, J. T., Marcy, G. W., et al. 2006, ApJ, 646, 505
Croll, B., Walker, G. A. H., Kuschnig, R., et al. 2006, AJ, 648, 607
Donati, J.-F., Semel, M., Carter, B. D., Rees, D. E., & Collier Cameron, A. 1997, MNRAS, 291, 658
Donati, J.-F., Collier Cameron, A., Semel, M., et al. 2003, MNRAS, 345, 1145
Donati, J.-F., Howarth, I. D., Jardine, M. M., et al. 2006, MNRAS, 370, 629
Fares, R., Donati, J.-F., Moutou, C., et al. 2009, MNRAS, 398, 1383
Gizis, J. E., Reid, I. N., & Hawley, S. L. 2002, AJ, 123, 3356
Greaves, J. S., Holland, W. S., Wyatt, M. C., et al. 2005, AJ, 619, L187
Hatzes, A. P., Cochran, W. D., McArthur, B., et al. 2000, ApJ, 544, L145
Janson, M., Reffert, S., Brandner, W., et al. 2008, A&A, 488, 771
Jeffers, S. V., & Donati, J.-F. 2008, MNRAS, 390, 635
Jeffers, S. V., Donati, J.-F., Alecian, E., & Marsden, S. C. 2011, MNRAS, 411, 1301
Jeffers, S. V., Barnes, J. R., Jones, H. R. A., et al. 2014, MNRAS, 438, 2717
Marsden, S. C., Petit, P., Jeffers, S. V., et al. 2014, MNRAS, 444, 3517
Metcalfe, T. S., Buccino, A. P., Brown, B. P., et al. 2013, ApJ, 763, L26
Morgenthaler, A., Petit, P., Morin, J., et al. 2011, Astron. Nachr., 332, 866
Morgenthaler, A., Petit, P., Saar, S., et al. 2012, A&A, 540, A138
Petit, P., Donati, J.-F., & Collier Cameron, A. 2002, MNRAS, 334, 374
Petit, P., Dintrans, B., Solanki, S. K., et al. 2008, MNRAS, 388, 80
Petit, P., Dintrans, B., Morgenthaler, A., et al. 2009, A&A, 508, L9
Piskunov, N., Snik, F., Dolgopolov, A., et al. 2011, The Messenger, 143, 7
Quillen, A. C., & Thorndike, S. 2002, ApJ, 578, L149
Rees, D. E., & Semel, M. D. 1979, A&A, 74, 1
Reiners, A., Shulyak, D., Anglada-Escudé, G., et al. 2013, A&A, 552, A103
Rueedi, I., Solanki, S. K., Mathys, G., & Saar, S. H. 1997, A&A, 318, 429
Skilling, J., & Bryan, R. K. 1984, MNRAS, 211, 111
Smith, M. A. 1983, PASP, 95, 268
Valenti, J. A., & Fischer, D. A. 2005, ApJ, 159, 141
van Leeuwen, F. 2007, A&A, 474, 653